Engineered filtration media for broad-spectrum contaminant removal in water treatment

Linda Mohamed Meziani[1] and Mathieu Lapointe[1]*
[1] University of Québec – École de technologie supérieure, Montréal, Québec, H3C 1K3, Canada
* Corresponding author

Abstract

Polymers and metals-functionalized media were assessed for their versatility and ability to remove both conventional and emerging contaminants for drinking water applications. We synthesized 25 functionalized media and evaluated their performance over 640 filtration experiments across diverse water matrices and contaminant classes. For the removal of total organic carbon, turbidity, nanoplastics, phosphorus, metals, and PFOS, the functionalized media consistently and markedly outperformed conventional unmodified sand – which remains widely used globally as the final barrier for contaminant interception in drinking water treatment. By lowering turbidity and TOC, the functionalized media could strengthen pathogen control – consistent with the use of filtered-water turbidity in Canadian, U.S., and European regulations as an operational indicator of filtration performance and microbial barrier integrity – while reducing disinfection-by-product precursor loads and downstream disinfectant demand. The functionalized media were also regenerable through a simple pH-adjusted washing procedure. This study further demonstrated that functionalization can be applied directly to the sand already used in drinking water treatment filters. Because the functionalized media retain the same grain-size distribution and filter-bed depth, existing sand filters can be upgraded without replacing the starting media or substantially modifying plant infrastructure. This retrofit strategy could therefore considerably reduce full-scale implementation costs while providing a practical pathway to enhanced treatment performance.

Keywords: drinking water production, sustainable treatment, advanced materials, functionalized surfaces, adsorption, coagulation, conventional contaminants, emerging contaminants, nanoplastics, PFAS.

Main

Granular-media filtration is the most widely used filtration process for drinking-water treatment worldwide and is central to the production of a major share of the world's drinking water; in Canada and the United States, available national surveys suggest that it serves approximately 70 % of the population[1–3]. The global degradation of natural waters by increasing anthropogenic stressors threatens drinking water supplies for large and small communities[4]. Certain contaminants, such as nitrates and metals, are subject to regulation due to their demonstrated effects on human health. Beyond these regulated contaminants, an increasing concern involves emerging contaminants, whose toxicity and environmental persistence are still not fully understood. These contaminants include per- and polyfluoroalkyl substances (PFAS), micro- and nanoplastics, certain pharmaceuticals, and trace metals[5–7]. Although present at low concentrations (from µg L^{-1} to ng L^{-1}), these contaminants pose significant risks to human health and aquatic ecosystems due to their persistence, toxicity, and bioaccumulative potential[6,8,9]. Moreover, some of these persistent contaminants are also refractory to conventional drinking water treatment processes, such as physicochemical treatment and Cl_2-based disinfection, which were not initially designed to target these persistent micropollutants[10,11]. The drinking water industry hence needs more efficient, versatile and advanced barriers against such contaminants.

The proposed metal (hydr)oxide and polymers–enriched filtration/adsorption media show strong potential for the removal of a wide range of contaminants while remaining cost-effective[12,13]. In contrast to media coated only with metals, as presented in previous studies, more heterogeneous and

polymers-metals-coated media could provide more pathways for contaminant interception. These cheap materials exhibit promising adsorption capacity for metals, phosphorus, and colloids[14–17], as well as for natural organic matter (NOM), nanoplastics, some long-chain PFAS[18–23], and disinfection by-product precursors[24–26]. The negatively charged contaminants adsorb onto metal (hydr)oxides, notably due to interactions with the hydroxyl groups and the positively charged sites on the surface of metal (hydr)oxides (e.g., FeOOH or Fe_2O_3)[27]. Iron-coated granular media have previously been investigated for the adsorption of natural organic matter (NOM), phosphorus, and metals[18,28]. However, the synthesis routes reported in these studies generally rely on the complete and energy-intensive thermal conversion of metal hydroxides (e.g., $Fe(OH)_3$) into oxides (e.g., Fe_2O_3) at temperatures exceeding 500 °C. In the present study, we introduce a distinct functionalization strategy involving the addition of very-high-molecular-weight carboxylated polymers to the media surface. Polymer incorporation provided two major benefits: it substantially reduced the temperature required for functionalization and, more importantly, markedly enhanced colloid retention during filtration compared with sand modified with only metals, i.e., without polymers (*cf* Fig. 2e).

In this study, two types of materials were tested: (1) conventional silica sand and (2) silica sand modified by coating polymers and iron-based (hydr)oxides, aiming to improve the removal of both regulated and emerging contaminants from two surface waters subject to multiple diffuse and point pressures[29,30], notably from the Saint Lawrence River, which supplies drinking water to nearly 50 % of Quebec's population[31]. In addition to water from the Saint Lawrence River, characterized by low turbidity and low total organic carbon content, the functionalized sand was tested on more complex water matrices, including more turbid surface water and wastewater with higher organic matter content. The potential of functionalized media was measured using filtration columns fed with raw water. Several operational conditions were investigated, including filtration rate, river water pH and temperature, coagulant concentration, and media regeneration. We synthesized and tested 25 functionalized media, with different metals and polymers surface coverage. The results showed: (i) the higher capacity and versatility of modified media to remove various contaminants, (ii) the influence of parameters such as pH, temperature, and grain size on removal efficiency, and (iii) the possibility of washing and regenerating the modified media. In contrast to conventional adsorbents used in granular filtration, such as granular activated carbon, the adsorption capacity of the functionalized media can be easily recovered by a simple pH-adjusted rinsing procedure, or by heating. This study contributes to optimizing drinking water treatment by proposing innovative, sustainable solutions compatible with existing infrastructure to address the growing challenge of emerging contaminants. By modifying the existing filter media rather than the infrastructure of drinking water treatment units, this approach could provide small municipalities with budget constraints and larger municipalities with a practical and cost-effective solution to improve drinking water treatment performance.

Results and Discussion

Fine (d_{50} of 280 µm) and coarse (d_{50} of 711 µm) filter media were synthesized through surface modification using metal (hydr)oxides in combination with organic polymers. Silica sand (Fig. 1a) was functionalized with different iron (hydr)oxides and a high-molecular-weight polyacrylamide (PAM). PAM was incorporated during the coating process to enhance iron retention on the sand surface, while also contributing to contaminant removal through particle entrapment, polymer bridging[32], ions binding with divalent cationic ions[33] on carboxyl ($–COO^-$) groups and hydrogen bonding on amide ($–NH_2$) groups of the PAM[34] . The addition of PAM during synthesis promoted the adsorption and retention of Fe-based precursors onto the media surface through polymer bridging, while heat-induced contraction of the polymer (polymer coiling, Fig. 1a) chains brought the iron species into closer contact with the silica grains before the $Fe(OH)_3$ precursor was converted into transitional iron (hydr)oxide phases. The coating of iron (hydr)oxides and PAM onto the silica surface

led to the formation of a thin layer of < 1 µm thickness (Fig. 1a), leaving the particle size of the media virtually unchanged. Additionally, it is expected the rough Fe–PAM coating enhanced particle retention by increasing interception, contact points, and resistance to hydrodynamic detachment[35,36]. These surface modifications were also reflected in the morphology of the coated media. Compared with conventional silica sand (Fig. 1e), the functionalized media exhibited a rougher and more heterogeneous surface, providing a larger reactive area for interactions with the target contaminants (Fig. 1f). Their enhanced removal performance resulted from the complementary roles of metal (hydr)oxides and polymer chains, which promoted the retention of dissolved and particulate contaminants, respectively (Fig. 1f). The adsorption capacity of the media was restored via pH-adjusted washing, as demonstrated by the comparison of performance before and after regeneration (Fig. 1b–d), indicating the recovery of surface sites previously occupied by retained contaminants. This recovery confirms the potential of the functionalized media for repeated use following a simple regeneration step.

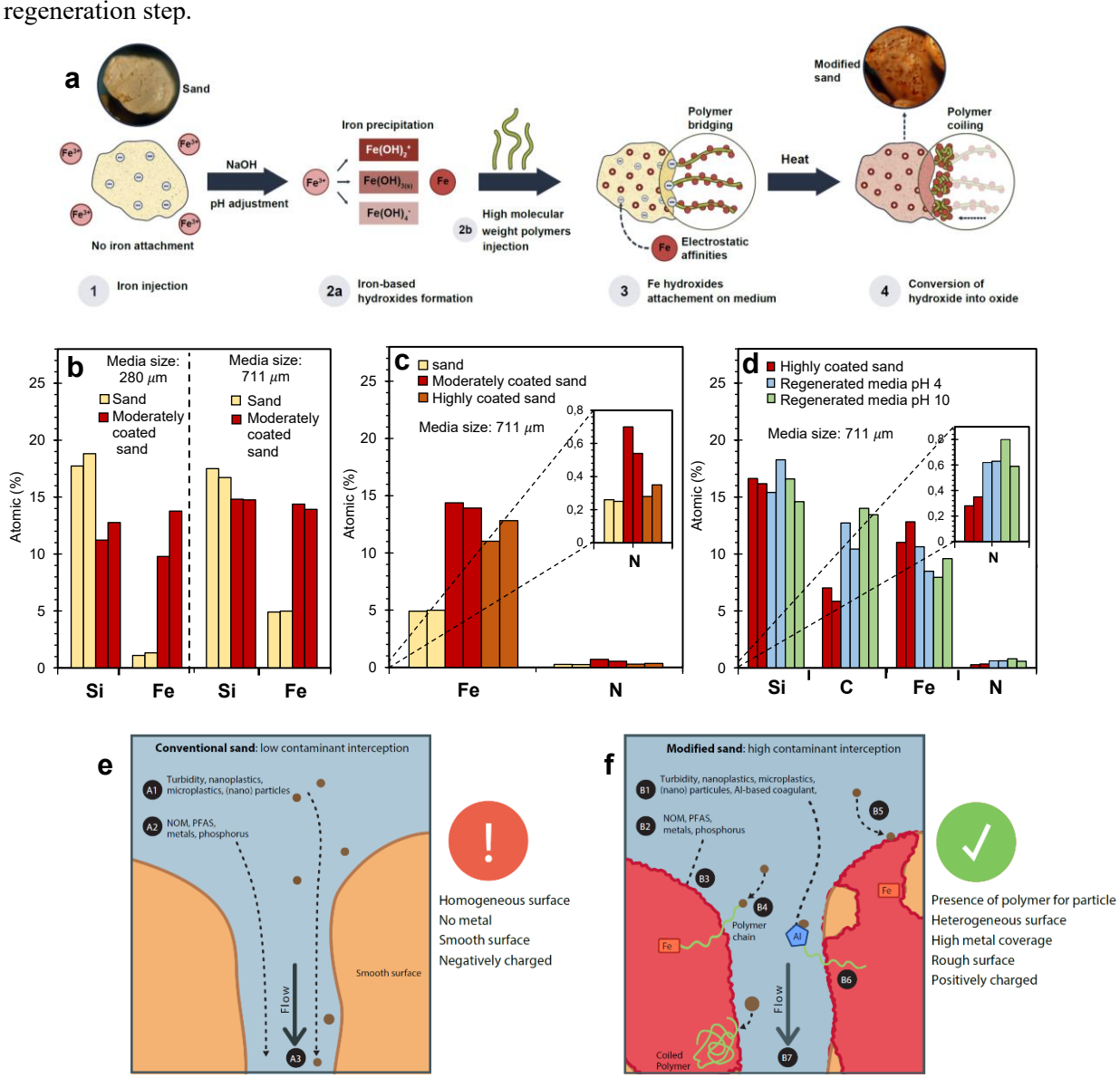

Fig. 1 | Synthesis and characterization of functionalized media. a. Synthesis of the modified media with iron and organic polymer. **b, c.** Elemental composition of different types of sand determined by XPS. **b**. The surface iron content increased, on average, from 1 % to 12 % for fine sand, and from 5 % to 14 % for coarse sand. **c.** XPS surface composition of moderately and highly coarse sand. **d**. XPS analysis of the surface composition of

coarse sand before and after 20 filtration cycles, followed by media regeneration at pH 4 and pH 10, showed that regeneration restored surface availability while retaining the Fe-based coating, with residual C and N remaining at the surface. XPS analysis was performed on duplicate samples. **e,f**. Expected mechanisms at play during contaminants interception with conventional vs. modified sand, adapted from Koumiya et al. (2026).

Optimization of the modified media synthesis

The impact of temperature (during hydroxide-oxide conversion, Fig1a, step 4), as well as polymer and iron concentrations during synthesis, was assessed . Coating temperature strongly influences the conversion and stabilization of the Fe-polymer complex on the media surface, hence the filtration performance. Sand dried at 90 °C shows the best results (~ 60 % turbidity reduction and > 95 % removal of TOC and 200 nm NPs), whereas a progressive loss of efficiency is observed above 200 °C, associated with the transformation of reactive amorphous phases into less active crystalline iron oxides (Fig. 2a–c) [27,37–39]. Filtrate pH also varies with coating temperature. In the first filtration cycle, media dried at lower temperatures produce slightly acidic filtrates, indicating proton release from unbonded Fe hydroxides such as $Fe(OH)^{2+}$ and $Fe(OH)_2^{+}$. At higher coating temperatures (> 350 °C), the progressive transformation into crystalline hematite (α-Fe_2O_3) reduces surface hydroxyl density and proton mobility, resulting in near-neutral filtrates due to lower surface reactivity (Fig. 2d)[40]. The addition of PAM strongly enhances turbidity removal (96 %) at an optimal loading of 0.28 mg PAM injected/g of sand. However, at a higher PAM loading (0.56 mg PAM injected/g of sand), efficiency decreases to 67 %, likely due to excess polymer causing surface overcoating and steric hindrance that limits particle capture (Fig. 2e)[41]. Fig. 2f shows that modified sand removes TOC (80–90 %) far more efficiently than unmodified sand (45 %) and the 0.45 µm filter (19 %), indicating that substantial fraction of TOC is dissolved. Without PAM, modified sand achieves ~ 92 % removal. Increasing PAM dosage reduces efficiency in TOC removal, likely due to electrostatic repulsion between negatively charged polymer layers and humic substances[33]. However, without PAM during the media modification, the turbidity removal was largely affected (15 %, Fig. 2e), hence indicating that adsorption via Fe (hydr)oxides is not the main mechanism for colloid retention. In that case, the role of PAM was essential and was expected to contribute to colloid retention via i) polymer bridging[32], ii) ions binding with divalent cationic ions[33] on carboxyl ($-COO^-$) groups and iii) hydrogen bonding on amide ($-NH_2$) groups of the PAM backbone[34]. The optimal PAM loading was hence a compromise between TOC removal and turbidity removal. Fig. 2g shows that residual iron in the filtrates remains below the drinking water limit (0.3 mg L^{-1})[42]. Fig. 2h shows that increasing iron content improves TOC and nanoparticle removal until a plateau is reached, consistent with the plateau in surface Fe observed by XPS (Fig. 1C).

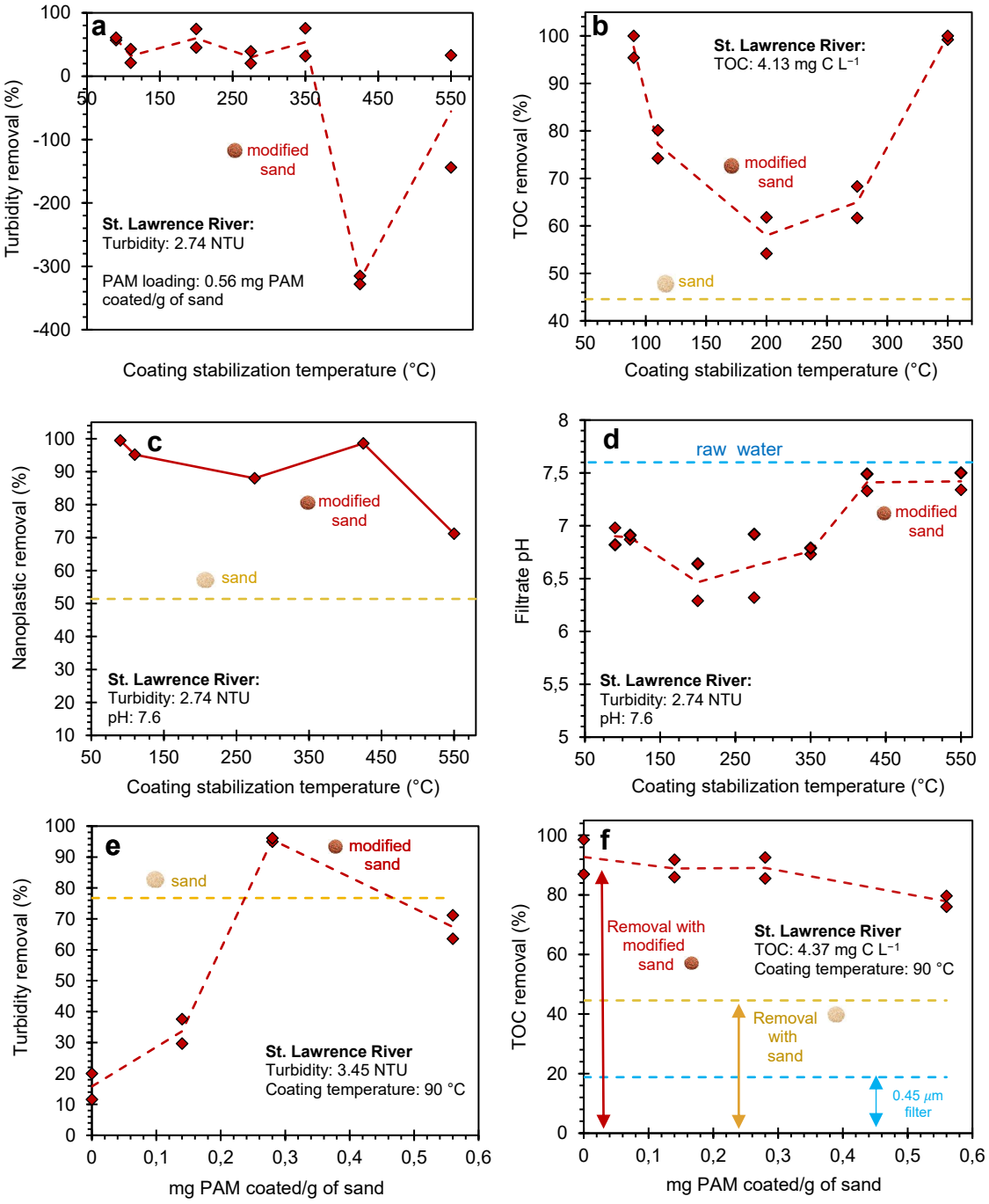
a
Turbidity removal (%)
modified sand
St. Lawrence River:
Turbidity: 2.74 NTU
PAM loading: 0.56 mg PAM coated/g of sand
Coating stabilization temperature (°C)
b
TOC removal (%)
St. Lawrence River:
TOC: 4.13 mg C L⁻¹
modified sand
sand
Coating stabilization temperature (°C)
c
Nanoplastic removal (%)
modified sand
sand
St. Lawrence River:
Turbidity: 2.74 NTU
pH: 7.6
Coating stabilization temperature (°C)
d
Filtrate pH
raw water
modified sand
St. Lawrence River:
Turbidity: 2.74 NTU
pH: 7.6
Coating stabilization temperature (°C)
e
Turbidity removal (%)
sand
modified sand
St. Lawrence River
Turbidity: 3.45 NTU
Coating temperature: 90 °C
mg PAM coated/g of sand
f
TOC removal (%)
Removal with modified sand
St. Lawrence River
TOC: 4.37 mg C L⁻¹
Coating temperature: 90 °C
Removal with sand
0.45 μm filter
mg PAM coated/g of sand

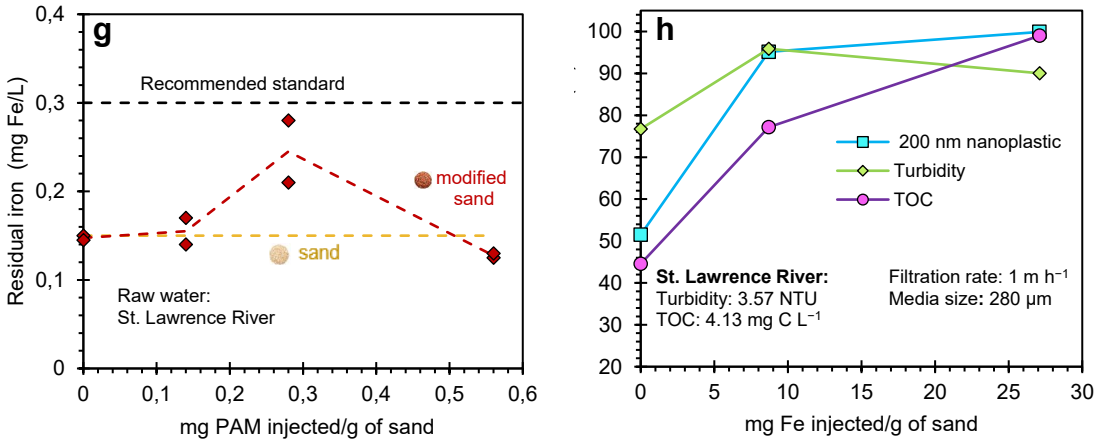

Fig. 2 | Optimization of functionalized media synthesis. Effect of coating temperature (90–550 °C) on **(a)** turbidity, **(b)** total organic carbon, **(c)** 200 nm nanoplastic, and **(d)** filtrate pH. Coating at 90 °C results in higher removal efficiency of both emerging and conventional contaminants. Impact of PAM loading (0–0.56 mg PAM injected/g of sand) on **(e)** turbidity and **(f)** TOC, with optimal removal achieved at 0.28 mg PAM injected/g of sand. **g.** Residual iron in the filtrate as a function of PAM loading (sand coating at 90 °C), in all experiments, residual Fe remained below the standard regulatory limit of 0.3 mg Fe L^{-1} (St. Lawrence River iron: 0.1 mg Fe L^{-1}). **h.** Effect of iron loading (0, 8.7 and 27.1 mg Fe injected/g of sand) on turbidity, TOC and nanoplastic 200 nm (sand coating at 110 °C). Conditions (a–g): Media size: 280 µm; moderately coated sand; filtration rate: 1 m h^{-1}; raw water pH 7.6. a–g, Dashed lines are included as eye guides connecting average values obtained from duplicate experiments.

Impact of modified media on emerging contaminants

The results presented in Fig. 3 show the influence of coagulant concentration, sand grain size, and media surface modification on the removal of emerging contaminants. Functionalized media retain nanoplastics more efficiently than conventional sand (Fig. 3a,b), achieving 83.5 % removal of 30 nm nanoplastics without alum, compared to only 24 % with conventional sand. The results are consistent with the enhanced adsorption capacity of modified granular surfaces reported previously[43]. The addition of alum decreased the removal of small 30 nm nanoplastics – known to be refractory to suboptimal coagulation[43] – with functionalized media (Fig. 3b), likely due to partial blockage of the media active sites. In contrast to refractory 30 nm nanoplastics, the removal of 200 nm nanoplastics was improved during coagulation (10 mg L^{-1} of alum; Fig. 3a), reaching 67 % removal with the functionalized sand compared to only 43 % with the conventional sand. These observations are consistent with previous studies mentioning the strong affinity of carboxylated polystyrene nanoplastics for iron (hydr)oxide surfaces through electrostatic interactions and ligand exchange with Fe-OH groups[44]. Fig.3 c–e show that nanoplastic removal depends on both particle size and media type. For 30 nm nanoplastics, removal increased from 90 % with conventional sand to 99.5 % with the functionalized media, whereas for 200 nm particles, removal increased from 69 % to 99 %, respectively. Functionalized media consistently outperform conventional sand across the tested media size (280–711 µm). Filtration performance decreased when larger media were used. These observations align with classical physicochemical filtration theory, in which decreasing media diameter increases particle–collector collision frequency and single-collector efficiency, as first described by Yao et al.[45] and later formalized by Tufenkji and Elimelech[46].

Fig. 3f illustrates PFOS removal using conventional sand, which is limited to 25 %, whereas the functionalized media achieve 46 % removal. As reported in previous studies, the enhanced PFOS retention likely resulted from the introduction of hydroxylated Fe sites capable of electrostatic and hydrogen-bonding interactions with the sulfonate headgroup[47,48]. These results are particularly relevant in the environmental context of the St. Lawrence River watershed, where PFOS accounts for

19 % of all PFAS detected in surface waters, as reported in the study by Teymoorian et al.[49]. The high proportion of PFOS among measured PFAS underscores the importance of implementing treatment processes specifically targeting some classes of PFAS.

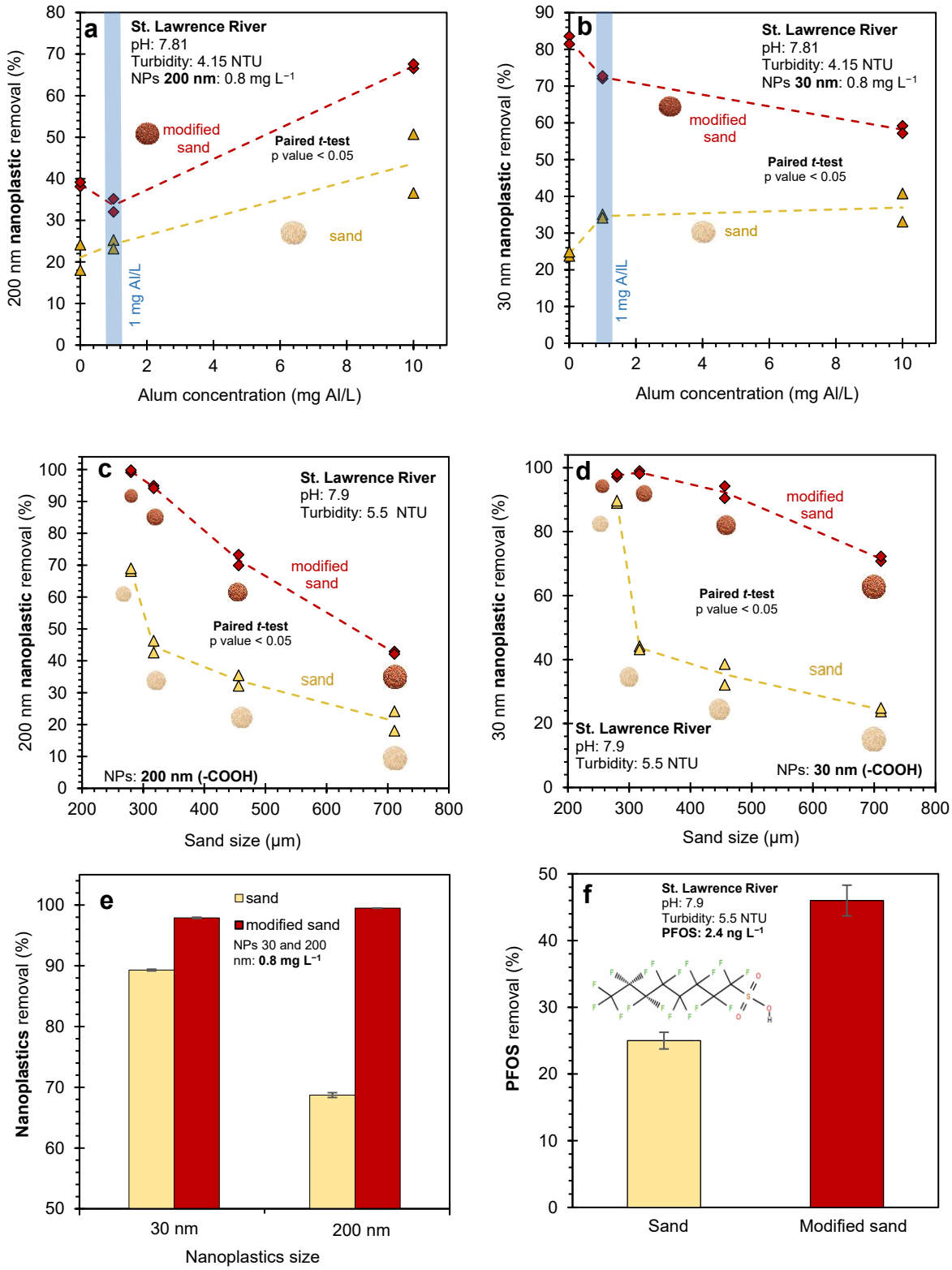

Fig. 3 | Nanoplastics and PFAS removal through different media. **a,b.** Removal of 200 nm **(a)** and 30 nm **(b)** nanoplastics as a function of alum concentration (0–10 mg Al L^{-1}) using conventional and functionalized sand. Media size: 711 µm, highly coated sand. **c,d.** Removal of 200 nm **(c)** and 30 nm **(d)** nanoplastics as a function of sand grain size (280–711 µm) using conventional sand and moderately coated sand. **e.** Removal of 30 and 200 nm nanoplastics by conventional sand and functionalized media (D_{50} = 280 µm; moderately coated). **f.** PFOS removal: 25 % conventional sand and 46 % with functionalized media (D_{50} = 711 µm; highly coated sand). Filtration rate (a–f): 1 m h^{-1}. c–f, Test were performance without coagulant. All experiments were performed in duplicate. a–d, Dashed lines are included as eye guides connecting average values obtained from duplicate experiments.

Impact of physicochemical treatment and filtration rate

To reduce head loss caused by fine sand, a coarse sand (711 µm) was used in subsequent experiments. Fig. 4a–c show a clear difference between the functionalized sand and the unmodified sand for the removal of turbidity, TOC and orthophosphates. At low alum concentration (≤ 1 mg Al L^{-1}), the versatile functionalized sand achieved high removal efficiencies for turbidity (> 90 %), TOC (~ 55–65 %), and orthophosphates (~ 40–50 %), whereas the unmodified sand required much higher alum concentrations for similar results (up to 20 mg alum L^{-1}). This indicates that the modified media actively promotes i) capture of colloids on the PAM structure, ii) organic molecules adsorption, and iii) the removal of negatively charged orthophosphates through electrostatic interactions with positively charged iron (hydr)oxide surfaces[26,50,51]. The reduction of TOC would limit the formation of by-products during subsequent water disinfection processes[52,53].

Filtration velocity influences TOC and turbidity removal efficiency. The fine modified sand exhibited higher removal efficiency than the fine conventional sand of the same grain size under the conditions investigated. For TOC (Fig. 4d), the moderately coated fine sand achieved approximately 93 % removal at 1 m h^{-1}, which decreased with increasing filtration velocity, likely owing to the reduced contact time. In comparison, the conventional fine sand achieved approximately 35 % removal under the same conditions. The highly coated coarse sand showed a more moderate decrease in removal efficiency, from 64 % to 47 % as filtration velocity increased. For turbidity (Fig. 4e,f), the modified fine sand also maintained higher removal efficiency than the conventional fine sand. At 7.5 m h^{-1}, removal reached approximately 61 % with the modified fine sand, compared to only 26 % for the conventional fine sand. Although removal decreased with increasing filtration velocity, consistent with previously reported observations for conventional sand filters[54], the removal efficiency remained substantially higher than that of the conventional sand. These results suggest that an iron-PAM functionalized medium could improve treated-water quality by maintaining lower turbidity – potentially strengthening the barrier against pathogens. They also suggest that higher filtration velocities could be achieved without significantly compromising turbidity removal, potentially offering an opportunity to increase the capacity of existing treatment facilities.

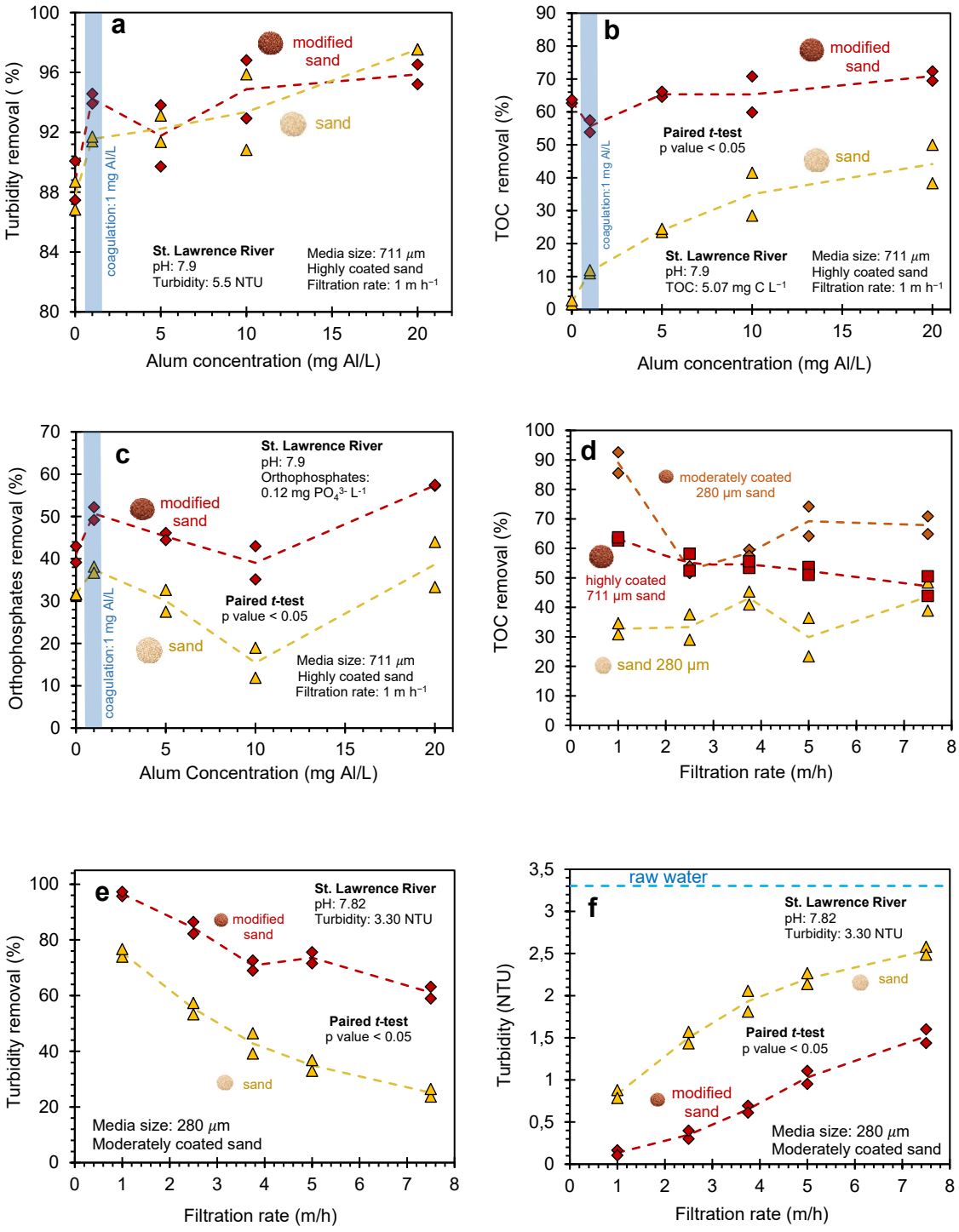

Fig. 4 | Impact of alum concentration, filtration rate, and sand particle size on the removal of conventional contaminants. a–c. Effect of alum concentration (0–20 mg Al L^{-1}) on **(a)** turbidity, **(b)** total organic carbon (TOC), and **(c)** orthophosphates removal for conventional and functionalized media. For both media, contaminant removal is highest at an alum concentration of 20 mg Al L^{-1}. **d–f.** Impact of filtration rate (1–7.5 m h^{-1}) on **(d)** TOC removal by conventional sand, moderately coated sand (280 µm) and highly coated sand (711 µm), **(e)** turbidity removal for conventional and functionalized fine sand, and **(f)** turbidity in water filtered through conventional fine sand and functionalized fine media. Both media filters show optimal performance at low filtration rates. Experimental conditions d: filtration rate: 1 m h^{-1}, experiments with 280 µm moderately coated

sand (St. Lawrence River water: pH 7.82, TOC 8.75 mg C L^{-1}), and with 711 µm highly coated sand (St. Lawrence River: pH 7.9, TOC 6.71 mg C L^{-1}). a–f, Dashed lines are included as eye guides connecting average values obtained from duplicate experiments.

Impact of pH and temperature

Turbidity removal showed minor variations with pH and temperature and was slightly higher for iron-modified sand, indicating that physical mechanisms dominate but can be influenced by surface chemistry (Fig. 5a,e). In contrast, total organic carbon (TOC) removal strongly depended on both the media type and the operation conditions. Iron-PAM-modified sand significantly enhanced TOC removal, peaking near neutral pH (~7–8) and at 20–25 °C, whereas unmodified sand remained inefficient and inconsistent (Fig. 5b,f). The decrease in TOC removal at lower temperatures could be attributed to slower adsorption kinetics and mass transfer (Fig. 5f). Higher temperatures may promote the diffusion of organic matter toward the adsorbent surfaces and enhance its removal[55]. Thus, lower temperatures may require longer contact times to achieve comparable removal. These findings demonstrate that chemical modification of sand can selectively improve TOC removal without the addition of a coagulant. Iron and copper removal as a function of pH are shown in Fig. 5c,d. The functionalized media outperformed unmodified sand, as pH-dependent changes in the charge of iron (hydr)oxides influenced metal ion binding, consistent with surface chemistry principles described by Kosmulski[56]. Residual iron concentrations (Fig. 5g) generally remained very low (<0.3 mg L^{-1}), an aesthetic guideline for drinking water in Canada[42]. Manganese concentrations (Fig. 5h) stayed well below the recent regulatory limit of 0.12 mg L^{-1} [57].

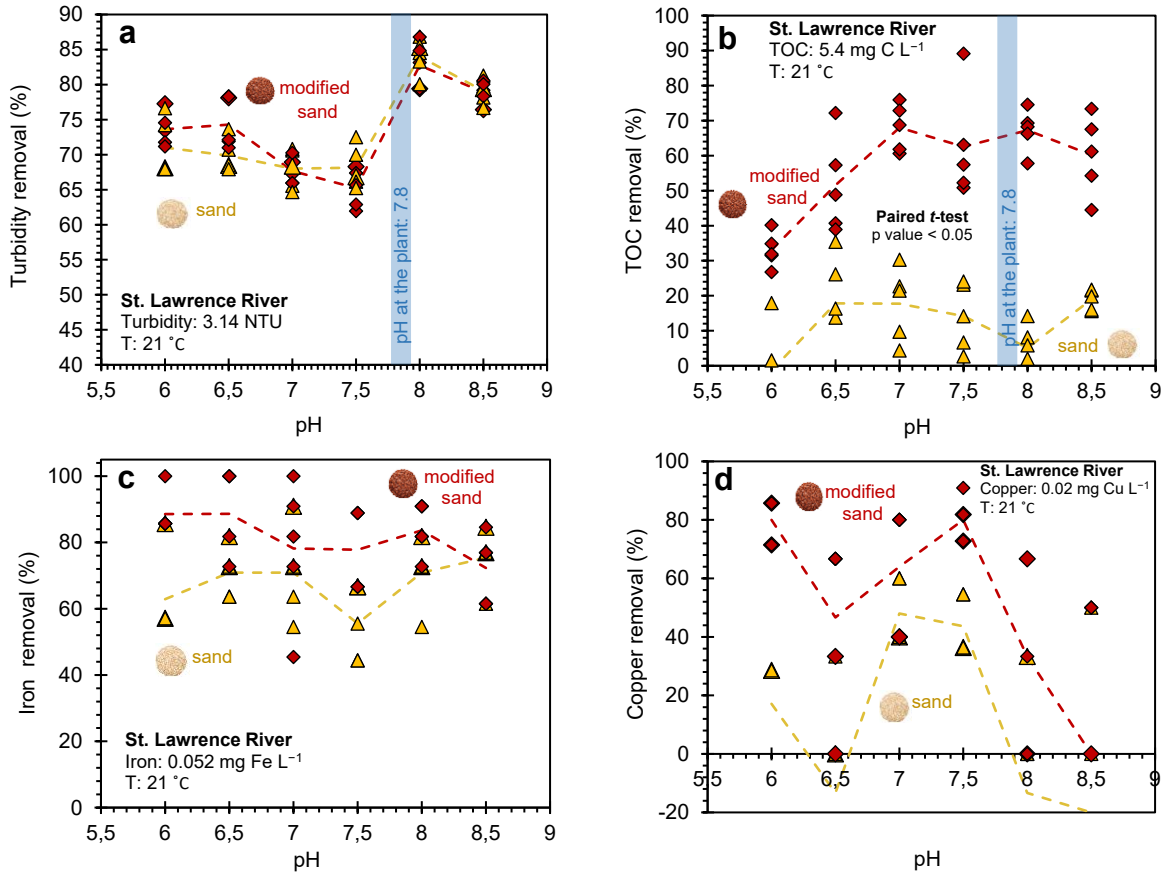

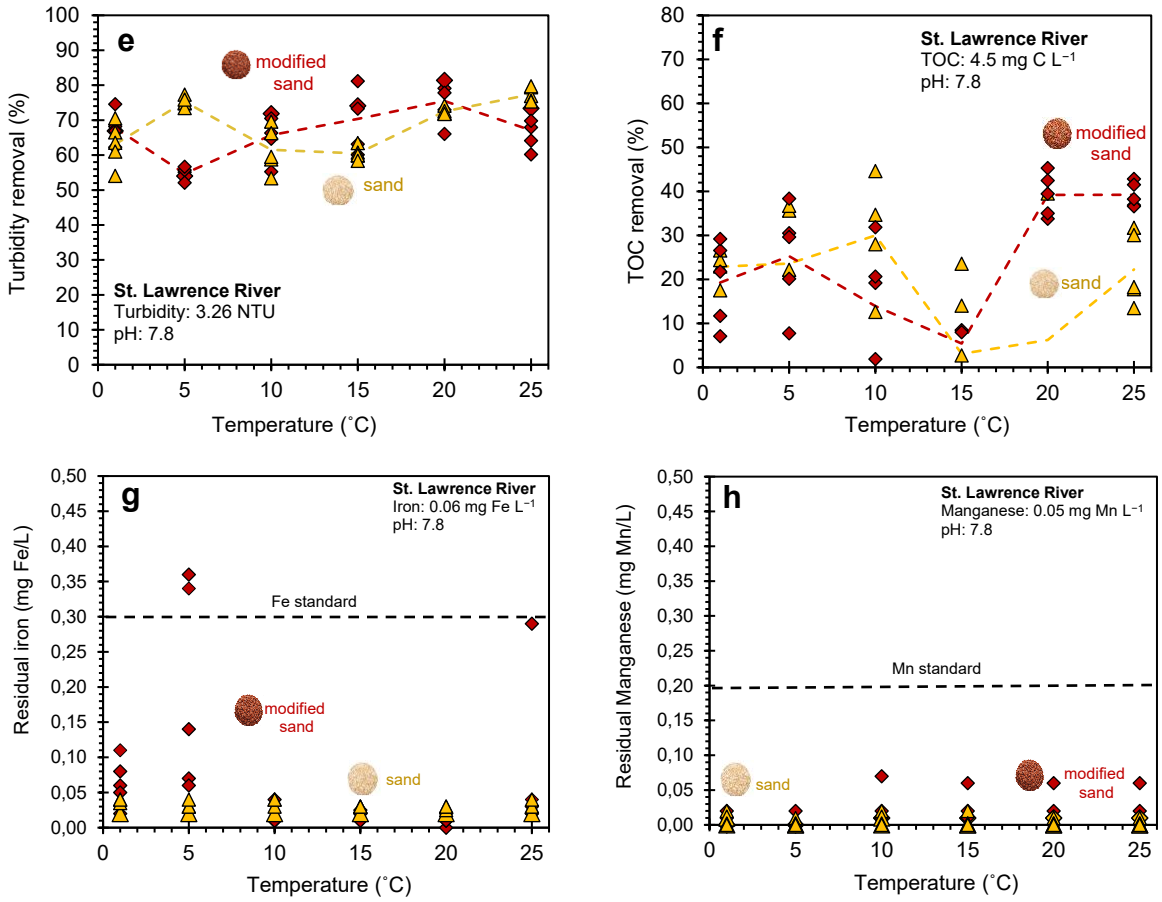

Fig. 5 | Effect of pH and temperature on the removal of conventional contaminants. a–d. Effect of river water pH variation (6–8.5) on removal of conventional contaminants. **(a)** turbidity, **(b)** total organic carbon (TOC), **(c)** iron and **(d)** copper removal for conventional and functionalized sand. **e–f.** Temperature dependent removal of turbidity **(e)** and TOC **(f)** from 1 to 25 °C**. g,h.** Residual iron **(g)** and manganese **(h)** concentrations in the treated water as a function of temperature. St. Lawrence River pH: 7.8. Overall, functionalized sand achieves higher contaminant removal and lower residual metal concentrations across most pH and temperature conditions. Conditions (a–h): Media size: 711 µm; highly coated sand; filtration rate: 1 m h^{-1}. a–h, Dashed lines are included as eye guides connecting average values obtained from duplicate experiments.

Advanced media can also be regenerated and reused

During the first 5 hours of filtration (20 cycles; step 1, Fig. 6c–f), TOC removal performance gradually decreased for both media, with this decline being more pronounced for the functionalized sand, suggesting a progressive occupation of the adsorption sites. This behavior is consistent with the XPS analyses (Fig. 6b) and previous studies reporting strong interactions between humic compounds and positively charged surfaces, which favor their adsorption and gradually lead to the saturation of active sites[58]. Despite this decrease, the functionalized sand exhibited higher TOC removal than the conventional sand, highlighting the combined contribution of chemical adsorption and physical filtration.

During the regeneration phase (Fig. 6a, g–j), the wash solutions from the functionalized sand showed higher TOC and turbidity concentrations, indicating more substantial desorption of the retained contaminants. This efficiency depends on the wash pH, which may be related to changes in the surface

charge of FeOOH near its point of zero charge, thereby altering its interactions with the contaminants[59]. Iron release was greater under alkaline conditions (Fig. 6j), consistent with the decrease in surface Fe content observed by XPS (Fig. 1d), emphasizing the need to rigorously adjust the wash pH to maximize desorption while preserving coating integrity.

Following regeneration, reuse of the media over five cycles (step 2, Fig. 6k–n) demonstrated a near-complete restoration of TOC and turbidity removal efficiencies under optimized pH conditions. This reversibility confirms that the washing protocol effectively frees the active sites. Overall, these results validate the robustness and high reuse potential of the functionalized sand for advanced filtration applications.

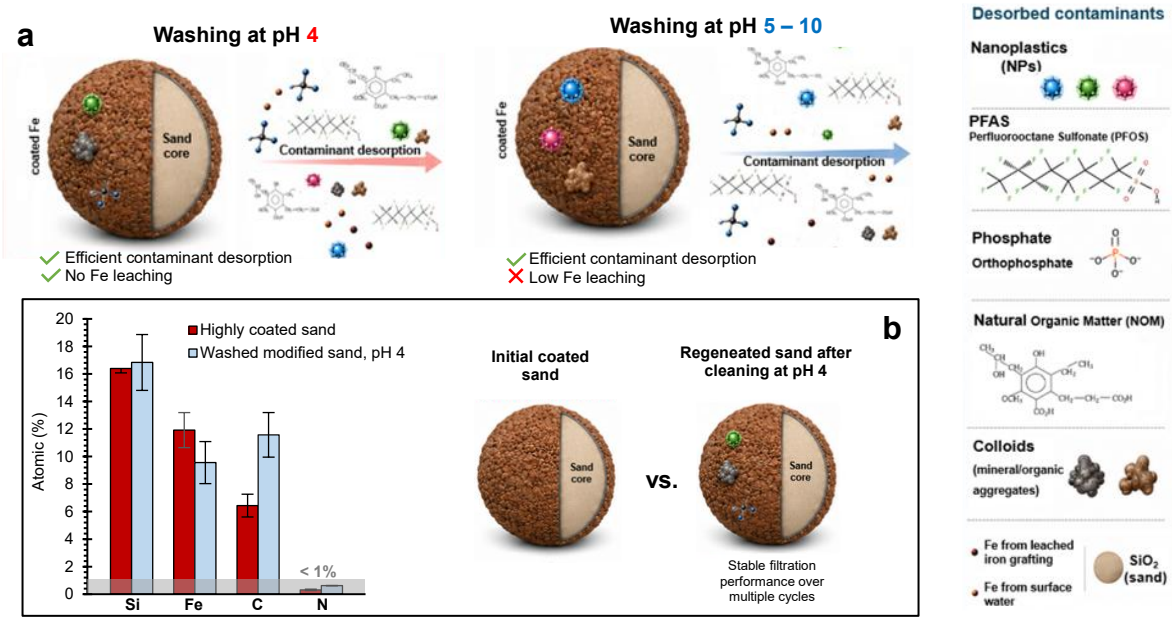

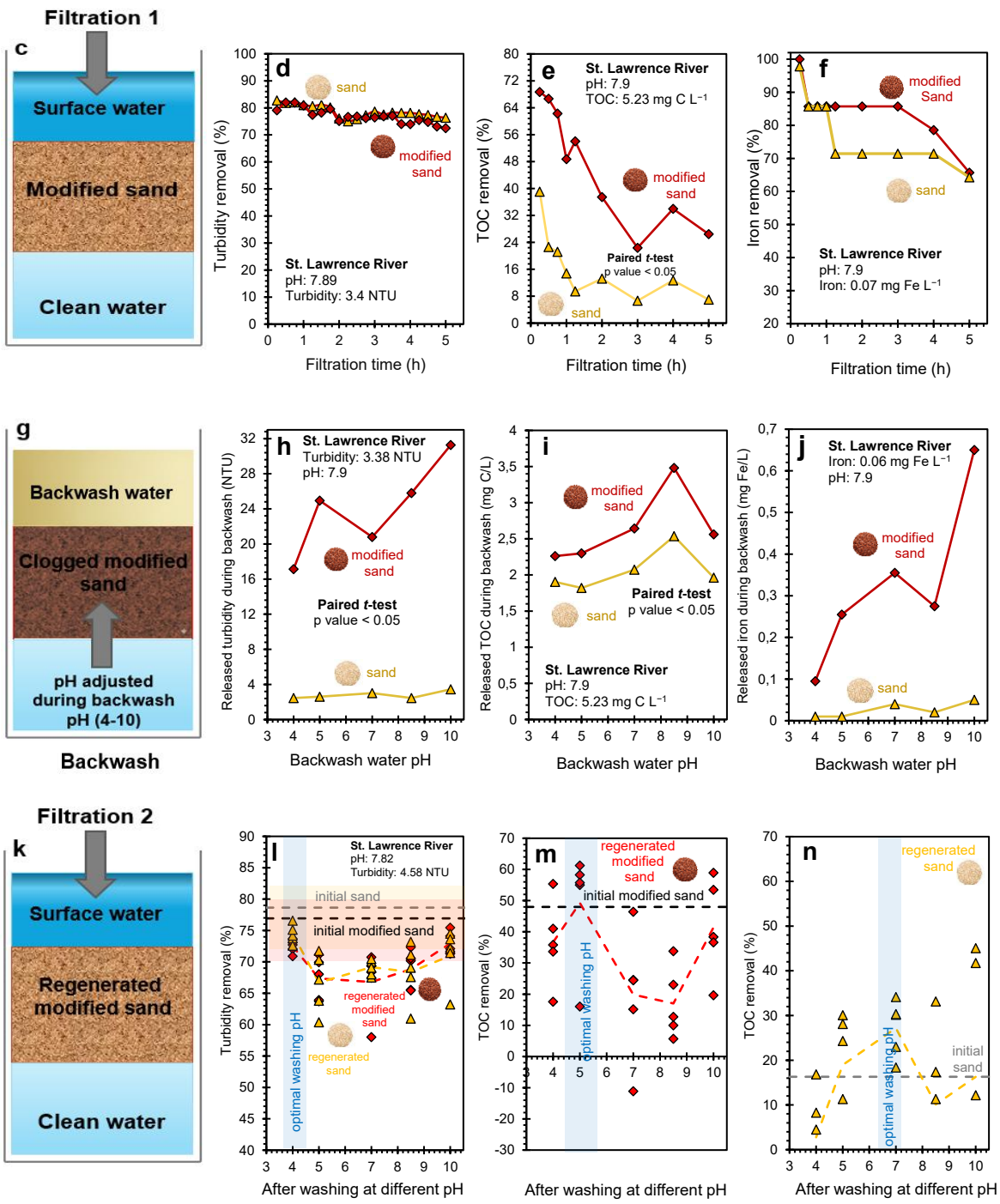
Filtration 1
c
Surface water
Modified sand
Clean water
d
sand
modified sand
St. Lawrence River
pH: 7.89
Turbidity: 3.4 NTU
Turbidity removal (%)
Filtration time (h)
e
St. Lawrence River
pH: 7.9
TOC: 5.23 mg C L⁻¹
modified sand
Paired t-test
p value < 0.05
sand
TOC removal (%)
Filtration time (h)
f
modified Sand
sand
St. Lawrence River
pH: 7.9
Iron: 0.07 mg Fe L⁻¹
Iron removal (%)
Filtration time (h)
g
Backwash water
Clogged modified sand
pH adjusted during backwash pH (4-10)
Backwash
h
St. Lawrence River
Turbidity: 3.38 NTU
pH: 7.9
modified sand
Paired t-test
p value < 0.05
sand
Released turbidity during backwash (NTU)
Backwash water pH
i
modified sand
Paired t-test
p value < 0.05
sand
St. Lawrence River
pH: 7.9
TOC: 5.23 mg C L⁻¹
Released TOC during backwash (mg C/L)
Backwash water pH
j
St. Lawrence River
Iron: 0.06 mg Fe L⁻¹
pH: 7.9
modified sand
sand
Released iron during backwash (mg Fe/L)
Backwash water pH
Filtration 2
k
Surface water
Regenerated modified sand
Clean water
l
St. Lawrence River
pH: 7.82
Turbidity: 4.58 NTU
initial sand
initial modified sand
regenerated modified sand
regenerated sand
optimal washing pH
Turbidity removal (%)
After washing at different pH
m
regenerated modified sand
initial modified sand
optimal washing pH
TOC removal (%)
After washing at different pH
n
regenerated sand
initial sand
optimal washing pH
TOC removal (%)
After washing at different pH

Fig. 6 | Media regeneration and stability. a. Schematic illustration of the desorption mechanism from a functionalized sand grain, showing contaminant detachment during washing at pH 4–10. **b.** XPS analyses showing the elemental composition of the virgin functionalized media and the regenerated functionalized media at pH 4. **c.** Schematic of filtration stage 1 operated over 20 cycles using functionalized media. **d–f.** Evolution of removal efficiencies for **(d)** turbidity, **(e)** total organic carbon (TOC), and **(f)** iron during filtration cycles. **g.** Schematic of the backwash process using solutions with pH ranging from 4 to 10. **h–j**. Effect of backwash pH on contaminant desorption: **(h)** turbidity in the backwash water, **(i)** TOC, and **(j)** iron concentration for both conventional sand and functionalized media. **k.** Schematic of filtration stage 2 using regenerated functionalized media over 5 cycles. **l–n.** Performance of regenerated media as a function of washing pH. a, was recreated using AI-assisted tools. All experiments were performed using highly coated sand, particle size of 711 µm and a filtration rate of 1 m h^{-1}.

Aggregated relation

Fig. 7a–c illustrates the relationship between turbidity removal and the removal of 30 and 200 nm nanoplastics at different concentrations of alum. For 30 nm particles (Fig. 7a) and 200 nm particles (Fig. 7b), increasing alum doses (0 to 20 mg Al L^{-1}) promotes the aggregation and capture of nanoplastics, thereby reducing data dispersion. Isolating the strong coagulation range (10–20 mg Al L^{-1}), by removing the coagulant-free points shown in the left panel and jointly excluding the 0 and 1 mg Al L^{-1} doses in the central panel, leads the results for both nanoplastic sizes to converge toward an excellent linear correlation *(*$r > 0.99$ for the modified sand and $r > 0.99$ for the unmodified sand). These results suggest that the relationship between turbidity and nanoplastic removal is not maintained under suboptimal coagulation conditions. These observations confirm that colloidal destabilization and incorporation into aluminum hydroxide flocs govern the behavior of nanoplastics during water treatment[60]. The impact of coagulation on the establishment of a linear relationship is highlighted by the convergence of the combined data for both particle sizes (Fig. 7c). By excluding the circled points in the left panel (0 mg Al L^{-1}), corresponding to the absence of coagulant, as well as the 0 and 1 mg Al L^{-1} doses in the central panel, the results converge toward a linear correlation ($r > 0.95$) (Fig. 7c–right panel). These conditions correspond to alum doses that are insufficient to ensure effective colloidal destabilization. For the full dataset, including filtration tests on unmodified and modified sand using synthetic 30 and 200 nm nanoplastics, the observed correlation supports the existence of a relationship between nanoplastic removal and the corresponding reduction in turbidity under controlled alum dosing conditions. Given the analytical challenges associated with their detection and quantification, turbidity reduction could serve as an indirect indicator of nanoplastic removal under controlled coagulation conditions.

Fig. 7d illustrates the removal of 30 and 200 nm nanoplastics by conventional sand and iron-modified sand in both surface water and wastewater. The results indicate that the functionalized medium remains effective even in highly contaminated environments, achieving a removal rate twice as high as that of unmodified sand. These data are consistent with the study by Koumiya et al.[61].

Overall, these results suggest that turbidity may serve as a reliable predictor of nanoplastics removal when coagulation conditions are sufficient to promote effective aggregation and floc formation, but not under suboptimal coagulation conditions where particle destabilization remains incomplete.

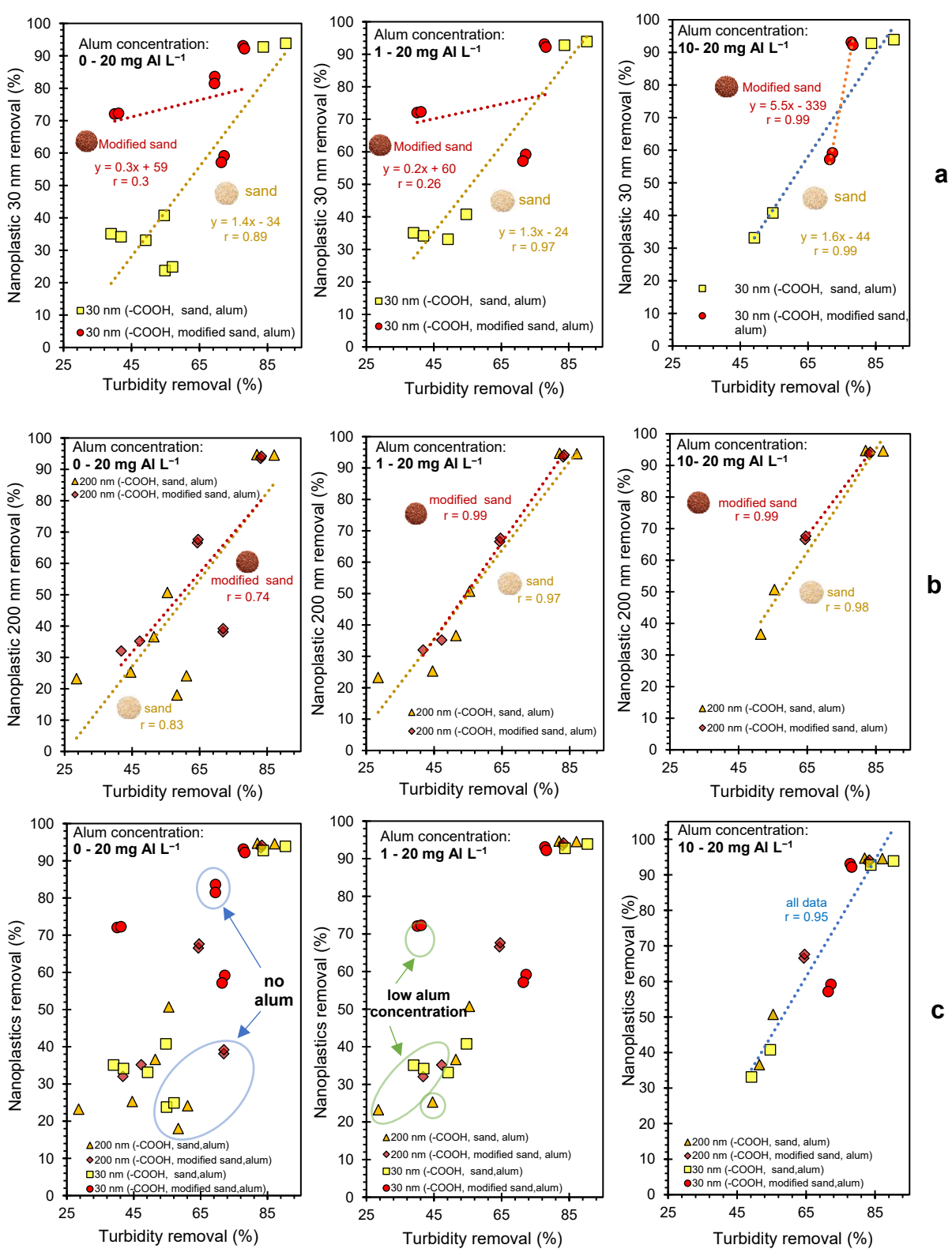
Alum concentration:
0 - 20 mg Al L⁻¹
Modified sand
y = 0.3x + 59
r = 0.3
sand
y = 1.4x - 34
r = 0.89
30 nm (-COOH, sand, alum)
30 nm (-COOH, modified sand, alum)
Nanoplastic 30 nm removal (%)
Turbidity removal (%)
Alum concentration:
1 - 20 mg Al L⁻¹
Modified sand
y = 0.2x + 60
r = 0.26
sand
y = 1.3x - 24
r = 0.97
Alum concentration:
10- 20 mg Al L⁻¹
Modified sand
y = 5.5x - 339
r = 0.99
sand
y = 1.6x - 44
r = 0.99
a
Nanoplastic 200 nm removal (%)
200 nm (-COOH, sand, alum)
200 nm (-COOH, modified sand, alum)
modified sand
r = 0.74
sand
r = 0.83
modified sand
r = 0.99
sand
r = 0.97
modified sand
r = 0.99
sand
r = 0.98
b
Nanoplastics removal (%)
no alum
30 nm (-COOH, sand,alum)
30 nm (-COOH, modified sand,alum)
low alum concentration
all data
r = 0.95
c

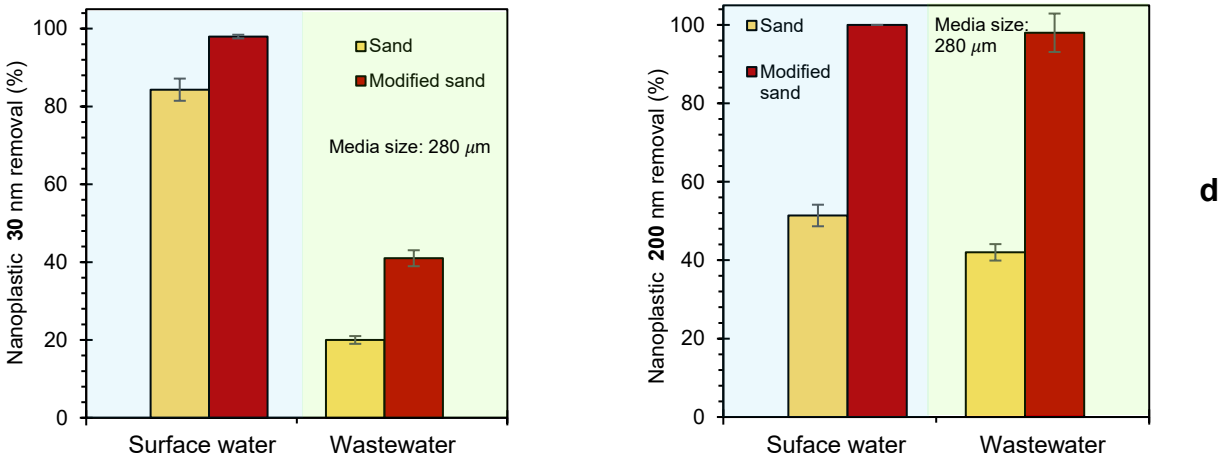

d

Fig. 7 | Correlation between the removal of polystyrene nanoplastics and turbidity under various treatment conditions. a. Fluorescent, carboxylate-functionalized 30 nm polystyrene nanoplastics subjected to coagulation with alum (0–20 mg Al L^{-1}). **b**. Fluorescent, carboxylate-functionalized 200 nm polystyrene nanoplastics coagulated with alum (0–20 mg Al L^{-1}). **c**. Simultaneous removal of fluorescent, carboxylate functionalized 30 nm and 200 nm polystyrene nanoplastics after coagulation with alum (0–20 mg Al L^{-1}). **d**. Removal efficiency of 30 and 200 nm polystyrene nanoplastics in St. Lawrence River water and wastewater as a function of turbidity reduction; heavily coated sand. In most experiments, turbidity decrease is strongly correlated with efficient nanoplastics removal. Experimental conditions (a–c), Media size: 711 μm; highly coated sand; filtration rate: 1 m h^{-1}; nanoplastic concentration: 0.8 mg NPs L^{-1}.

Conclusion

Functionalization of sand significantly improves the performance of conventional granular filtration by enabling the versatile adsorption of a broad range of regulated and emerging contaminants, including turbidity, nanoplastics, metals, and total organic carbon (TOC). The positively charged surface sites further enhance the removal of per- and polyfluoroalkyl substances (PFAS), particularly perfluorooctane sulfonate (PFOS).

The functionalized media maintained enhanced removal performance across a wide range of operating conditions, including variations in filtration rate, temperature, pH, coagulation conditions, and media size. This resilience highlights the potential of the modified media to provide more consistent treatment performance under variable water treatment conditions. The column experiments further demonstrated effective treatment across different water matrices, achieving low turbidity and TOC concentrations even at low coagulant dosages.

XPS analyses following washing at pH 4 indicate contaminant desorption without significant iron loss.

From an application perspective, these results highlight the potential of functionalized media as a simple, cost-effective, and efficient solution for surface water treatment. In contrast to membrane-based technologies, this material is low-cost, scalable, and easy to operate, as it relies solely on the modification of existing sand without requiring major changes to infrastructure.

The column-scale results obtained in this study provide the basis for ongoing pilot-scale testing using 3-inch columns operated under conditions representative of the Des-Baillets drinking water treatment plant, which could treat approximately 1,000,000 m^3 of water per day. These ongoing pilot experiments will further assess the performance and operational feasibility of the functionalized media under conditions closer to full-scale operation.

Future work should also investigate the functionalized media's long-term performance in full-scale applications. Such advanced filtration media could provide enhanced public health protection by reducing the concentrations of various chemical contaminants and pathogens, while also limiting the formation of disinfection by-products. This work is expected to stimulate further discussion and encourage additional research into innovative media modifications and advanced filtration strategies.

Materials and Methods

Chemicals and materials

Water matrices and characterization

The St. Lawrence River (surface water 1) served as the primary matrix for this study. Surface water was collected at Promenade-de-Bellerive Park (Montreal, Canada; 45.595° N, 73.509° W) during two distinct sampling campaigns conducted in October 2023 and May 2024. To further validate the applicability of the method across varying water qualities, two additional matrices were employed for comparative testing: surface water from Beaudet Reservoir (surface water 2) and a wastewater effluent (WW). While the experimental campaign focused predominantly on St. Lawrence water, the surface 2 and WW samples provided contrasting levels of turbidity and organic loading for robustness testing. All matrices were stored at 4 °C in climate-controlled chambers and thoroughly homogenized before use. The key physicochemical parameters for the three matrices, representing the range of values observed during the study, are summarized in Table 1.

Table 1: Physicochemical characterization of the St. Lawrence River water and comparative matrices

Parameter	Surface water 1	Surface water 2	WW
pH	7.6–7.9	7.4 ± 0.3	6.8 ± 0.2
Turbidity (NTU)	2.74–5.5	10.6 ± 0.5	54.1
TOC (mg C/L)	3.4–6.8	8.2–11.6	10.8

Synthesis of functionalized media

The functionalized media were developed by chemical modification of the surface of raw silica sand to enhance the simultaneous removal of regulated and emerging contaminants. The synthesis protocol was standardized across different sand types and sizes.

Precipitation and polymer-aided coating

Briefly, 180 g of conventional sand (D_{50} = 280 µm) was suspended in 100 mL of deionized water, and 8 mL of ferric chloride solution (PIX 311, 13.36 % Fe, Kemira Water Solutions Canada) was added under constant agitation. The addition of the $FeCl_3$ solution induces a strong acidification of the medium due to the hydrolysis of Fe^{3+} ions, as described by Benjamin et al.[28].

$$Fe^{3+} + nH_2O \longrightarrow Fe(OH)_n^{3-n} + nH^+ \quad (1)$$

To induce the precipitation of metallic hydroxides onto the sand surface, the solution pH was incrementally adjusted to 7.5 using 2N NaOH. To facilitate the deposition and stabilization of iron species, 100 mL of an anionic polyacrylamide (PAM) solution was introduced in two stages, followed by 5 min of homogenization. The PAM solution was prepared by dissolving 0.1 g of anionic PAM (Hydrex 3511, molecular weight > 10^6 g/mol, anionic charge density < 10 %) in 200 mL of deionized water and stirring at room temperature for 15 min.

Thermal treatment and phase transformation

After decanting the supernatant, the coated sand was transferred to aluminum trays and underwent thermal annealing at 90 °C for 24 h. This process promotes the chemical coating of iron species and the phase transformation of the initial amorphous iron (hydr)oxides into stable, semi-crystalline oxyhydroxides, such as goethite (α-FeOOH), following a dehydration mechanism[27].

$$Fe(OH)_{3(s)} \xrightarrow{\Delta\,(90°C)} FeOOH_{(s)} + H_2O_{(g)} \qquad (2)$$

This moderate temperature of 90 °C ensures the formation of robust siloxane-iron bonds (≡ Si-O-Fe) while preserving the structural integrity of the PAM flocculant. The resulting media was washed thrice with deionized water (pH 7.5) to remove loosely bound particles and dried again under similar conditions.

Surface properties and characterization

This coating procedure generates positively charged metallic surface sites, enhancing the adsorption capacity for negatively charged species, including dissolved organic matter, nanoplastics (NPs), and per- and polyfluoroalkyl substances (PFAS) via electrostatic interactions and ligand exchange mechanisms.

The particle size distribution of the sands was measured using a Mastersizer Malvern 3000. Five measurements were performed for each sand, and the mean D_{50} value was used to represent the characteristic particle size.

Table 2: Characteristics of the sand used

Sand type	D_{10} (µm)	D_{50} (µm)	D_{90} (µm)
Sand A	175	280	439
Sand B	255	317	391
Sand C	338	456	616
Sand D	457	711	919
Sand E	267	464	642

Optimization of Operating Parameters

Several trials were carried out to develop a high-performance functionalized medium. Table 3 summarizes the ranges of the parameters tested and the corresponding optimal values identified for each condition.

Table 3: Optimization of experimental conditions for the synthesis of the medium

Parameter	Value tested	Optimal value (D_{50} = 280 µm	Optimal value (D_{50} = 711 µm
Iron volume (mL)	8, 12, 25	8	12
PAM volume (mL)	0, 50, 100,150, 200	100	150
Drying temperature (°C)	90, 110, 200, 275, 350, 425, 550	90	90

The optimal operating parameters were determined by a systematic evaluation of the treated water, based on contaminant removal, neutral pH, and minimal iron leaching, compared to unmodified sand.

The surface modification was characterized by X-ray photoelectron spectroscopy (XPS) (Escalab 250Xi, Thermo Fisher Scientific). This technique made it possible to determine the surface composition of the porous media (silica sand and functionalized sand) and to confirm the presence of iron, thus attesting to the effectiveness of the modification process. Atomic percentages (Atomic %) were calculated from the peak areas after background subtraction, then corrected using the manufacturer's sensitivity factors and normalized with respect to the total detected signal.

Column Filtration Experiments

Synthesis efficiency was evaluated through column filtration experiments using a cylindrical glass column (AC 16/20, Cytiva; L = 20 cm, inner diameter = 1.5 cm), with a length-to-diameter ratio greater than 4 to minimize transverse dispersion[62]. The column was fitted with upper and lower adapters (AC, Cytiva), and an 80 µm mesh sieve was placed at the bottom of the lower adapter to prevent loss of the filter bed. For each experiment, 26 g of porous medium were packed into the column. A gentle vibration was applied for 30 s to remove trapped air and ensure homogeneous bed compaction. The upper adapter was connected to a syringe containing 50 mL of surface water, while the lower adapter directed the filtered water into a glass beaker for collection. Prior to filtration, the system was conditioned by flushing three times with ultrapure water (pH 7.5) to remove loosely bound particles and impurities from the unmodified sand. The syringe was mounted on a Kd Scientific syringe pump, delivering the influent at a constant flow rate of 3 mL min^{-1}. The number of filtration cycles varied depending on the parameters investigated (1, 5, or 20 cycles) for both unmodified and functionalized sand. Experiments conducted at one cycle were performed in duplicate. The pH and turbidity of the samples were measured on the same day using a pH meter (pH/CON 510 Series, Oakton) and a turbidimeter (HACH TL 2350), respectively.

Overall, more than 640 filtration experiments were conducted using different synthesized media formulations, conventional sand, and diverse water matrices, covering a broad range of operating conditions, contaminant classes, and regeneration conditions.

Parameters Influencing the Efficiency of the Functionalized Filter Media

Several experiments and analyses were conducted under different operating conditions to evaluate the efficiency and stability of the functionalized media. Table 4 summarizes the parameters investigated for both the functionalized media and the unmodified sand. For each condition, the filtered water was analyzed to determine the removal efficiency of the targeted contaminants.

Table 4: Operating parameters influencing the performance of the filter media

Parameter	Coagulant concentration (mg Al/L)	Surface water pH	Surface water temperature (°C)	Filtration rate (m/h)	Sand particle size (µm)
Tested value	0, 1, 5, 10, 20	6, 6.5, 7, 7.5, 8, 8.5	1, 5, 10, 15, 20, 25	1, 2.5, 3.75, 5, 7.5	280, 317, 456, 711
Analyses performed	Turbidity, TOC, PFAS, NPs, PO_4^{3-}, metals, residual iron	Turbidity, TOC, metals, residual iron	Turbidity, TOC, metals, residual iron	Turbidity, TOC, metals, residual iron	Turbidity, TOC, NPs, PO_4^{3-}, metals, residual iron

Regeneration of the Functionalized Media

Media regeneration was performed using a pH-controlled washing protocol to promote contaminant desorption while preserving coated iron. The media were first loaded through 20 filtration cycles using river water. This procedure was repeated five times to obtain independent batches for each material. The contaminated media were then washed by rinsing with 1.2 L of pH-adjusted solution (pH 4–10) under gentle stirring (1 min), followed by settling (30 s). The supernatant was collected for analysis. The washing efficiency was evaluated by measuring pH, turbidity, total organic carbon (TOC), and residual iron in the supernatant (Table 5). To assess the stability of the surface modification, selected samples regenerated at extreme pH conditions (pH 4 and 10) were further characterized by X-ray Photoelectron Spectroscopy (XPS).

Table 5: Washing conditions and analytical parameters

Medium	Backwash water pH	Analyzed parameter
Unmodified sand	4, 5, 7, 8.5, 10	pH, turbidity, TOC, residual iron
Functionalized media	4, 5, 7, 8.5, 10	pH, turbidity, TOC, residual iron

Reuse of the Regenerated Medium

Following regeneration, five filtration cycles of surface water were performed using the regenerated media. Five samples of unmodified sand and five samples of functionalized sand, regenerated at pH 4, 5, 7, 8.5, and 10, respectively, were evaluated to assess the durability and contaminant removal efficiency of the functionalized medium after regeneration. The filtered water was analyzed for turbidity, total organic carbon (TOC), and metals. For all experiments, unmodified sand was included as a control to allow direct comparison with the functionalized medium.

Nanoplastics, Orthophosphates, Total Organic Carbon and metals measurement

Two sizes of synthetic fluorescent nanoplastics, 30 and 200 nm (excitation/emission: 365/415 nm), were tested. The stock solution was diluted to 100 ppm in ultrapure water, and 0.8 mL of this solution was added to 100 mL of raw water to achieve a final concentration of 0.8 ppm. The concentration of nanoplastics in both raw and filtered water was measured using a fluorescence spectrophotometer (Eclipse, VARIAN).

Orthophosphates were determined using a spectrophotometer (Cary 300 Bio, VARIAN), and total organic carbon (TOC) content was measured with a carbon analyzer (FormacsHT, SKALAR). Metal concentrations were measured by inductively coupled plasma optical emission spectroscopy (ICP-OES, 5110; Agilent Technologies). A multi-element standard (AQ0-223-845, SCP SCIENCE) was used for ICP-OES calibration.

Authorship contribution statement

Linda Mohamed Meziani: Conceptualization, Methodology, Validation, Formal analysis, Investigation, Data Curation, Visualization, Writing - Original Draft.
Mathieu Lapointe: Conceptualization, Methodology, Validation, Formal analysis, Investigation, Resources, Data Curation, Writing, Review & Editing, Visualization, Supervision, Project administration, Funding acquisition.

Declaration of Competing Interest

M.L. has applied for a patent on the use of functionalized media for water treatment. The remaining authors declare no competing interests.

Acknowledgments

The authors acknowledge the assistance provided by Water Engineering and Environmental Processes Laboratory (LGEPE) at École de technologie supérieure (University of Québec). The authors also acknowledge the financial support from the Canada Research Chairs program (CRC-2024-00143), the Natural Sciences and Engineering Research Council of Canada (NSERC) Discovery Grants program (RGPIN-2023-03486), and the Ministère de l'Économie, de l'Innovation et de l'Énergie (MEIE, PSO program; AXE – 0446). The authors acknowledge IMPAKT Scientifik (Québec, Canada) for image editing. Walid Himeur and Nour Dine Mohamed El Bar are also thanked for their contributions to experimental work.

References

1. LeChevallier, M. W. Water Treatment and Pathogen Control: Process Efficiency in Achieving Safe Drinking Water. (Published on behalf of the World Health Organization by IWA Pub, London, 2004).
2. Statistics Canada. Survey of Drinking Water Plants, 2005 to 2007. Catalogue no. 16-403-X (Statistics Canada, 2009).
3. U.S. Environmental Protection Agency. 2006 Community Water System Survey Volume 1: Overview. EPA 815-R-09-001 (2009).
4. Schwarzenbach, R. P. *et al.* The Challenge of Micropollutants in Aquatic Systems. *Science* **313**, 1072–1077 (2006).
5. Cousins, I. T. *et al.* The concept of essential use for determining when uses of PFASs can be phased out. *Environ. Sci. Process. Impacts* **21**, 1803–1815 (2019).
6. Adeola, A. O., Paramo, L., Fuoco, G. & Naccache, R. Emerging hazardous chemicals and biological pollutants in Canadian aquatic systems and remediation approaches: A comprehensive status report. *Sci. Total Environ.* **954**, 176267 (2024).
7. Ayala Cabana, L., De Santiago-Martín, A., Meffe, R., López-Heras, I. & De Bustamante, I. Pharmaceutical and Trace Metal Interaction within the Water–Soil–Plant Continuum: Implications for Human and Soil Health. *Toxics* **12**, 457 (2024).
8. Habumugisha, T. *et al.* Toxicological review of micro- and nano-plastics in aquatic environments: Risks to ecosystems, food web dynamics and human health. *Ecotoxicol. Environ. Saf.* **278**, 116426 (2024).
9. Wang, C., Magnuson, J. T., Zheng, C. & Qiu, W. Incidence of pollution, bioaccumulation, biomagnification, and toxic effects of per- and polyfluoroalkyl substances (PFAS) in aquatic ecosystems: A review. *Aquat. Toxicol.* **286**, 107469 (2025).
10. Appleman, T. D. *et al.* Treatment of poly- and perfluoroalkyl substances in U.S. full-scale water treatment systems. *Water Res.* **51**, 246–255 (2014).
11. Luo, Y. *et al.* A review on the occurrence of micropollutants in the aquatic environment and their fate and removal during wastewater treatment. *Sci. Total Environ.* **473–474**, 619–641 (2014).
12. Callegari, A., Ferronato, N., Rada, E. C., Capodaglio, A. G. & Torretta, V. Assessment of arsenic removal efficiency by an iron oxide-coated sand filter process. *Environ. Sci. Pollut. Res.* **25**, 26135–26143 (2018).
13. Haouti, R. E. *et al.* Removal of heavy metals and organic pollutants by a sand rich in iron oxide. *Euro-Mediterr. J. Environ. Integr.* **3**, 17 (2018).

14. Thirunavukkarasu, O. S., Viraraghavan, T. & Subramanian, K. S. Arsenic Removal from Drinking Water using Iron Oxide-Coated Sand.
15. Charbonnet, J. A., Duan, Y. & Sedlak, D. L. The use of manganese oxide-coated sand for the removal of trace metal ions from stormwater. *Environ. Sci. Water Res. Technol.* **6**, 593–603 (2020).
16. Chardon, W. J., Groenenberg, J. E., Vink, J. P. M., Voegelin, A. & Koopmans, G. F. Use of iron-coated sand for removing soluble phosphorus from drainage water. *Sci. Total Environ.* **815**, 152738 (2022).
17. Khiadani, M., Zarrabi, M. & Foroughi, M. Urban runoff treatment using nano-sized iron oxide coated sand with and without magnetic field applying. *J. Environ. Health Sci. Eng.* **11**, 43 (2013).
18. Lapointe, M., Jahandideh, H., Alimi, O. S., Farner, J. M. & Tufenkji, N. Sustainable granular materials improve removal of natural organic matter, turbidity and microplastics during adsorption, ballasted flocculation and granular filtration. *J. Environ. Chem. Eng.* **13**, 116012 (2025).
19. Choe, Y., Won, J. & Burns, S. E. Impact of particle size and oxide phase on microplastic transport through iron oxide-coated sand. *Water Res.* **271**, 122856 (2025).
20. Johnson, R. L., Anschutz, A. J., Smolen, J. M., Simcik, M. F. & Penn, R. L. The Adsorption of Perfluorooctane Sulfonate onto Sand, Clay, and Iron Oxide Surfaces. *J. Chem. Eng. Data* **52**, 1165–1170 (2007).
21. Chaudhary, A. *et al.* Heavy-Metal Ions Control on PFAS Adsorption on Goethite in Aquatic Systems. *Environ. Sci. Technol.* **58**, 20235–20244 (2024).
22. Ordonez, D., Valencia, A., Sadmani, A. H. M. A. & Chang, N.-B. Green sorption media for the removal of perfluorooctanesulfonic acid (PFOS) and perfluorooctanoic acid (PFOA) from water. *Sci. Total Environ.* **819**, 152886 (2022).
23. Teng, B. *et al.* Study on PFAS removal by different forms of iron-modified biochar: Adsorption effects and catalytic activity. *J. Environ. Chem. Eng.* **13**, 120333 (2025).
24. Kaplan Bekaroglu, S. S., Yigit, N. O., Karanfil, T. & Kitis, M. The adsorptive removal of disinfection by-product precursors in a high-SUVA water using iron oxide-coated pumice and volcanic slag particles. *J. Hazard. Mater.* **183**, 389–394 (2010).
25. Korshin, G. V., Benjamin, M. M. & Sletten, R. S. Adsorption of natural organic matter (NOM) on iron oxide: Effects on NOM composition and formation of organo-halide compounds during chlorination. *Water Res.* **31**, 1643–1650 (1997).
26. Lapointe, M., Jahandideh, H., Farner, J. M. & Tufenkji, N. Super-bridging fibrous materials for water treatment. *Npj Clean Water* **5**, 11 (2022).

27. Cornell, R. M. & Schwertmann, U. *The Iron Oxides: Structure, Properties, Reactions, Occurrences and Uses*. (John Wiley & Sons, 2006).
28. Benjamin, M. M., Sletten, R. S., Bailey, R. P. & Bennett, T. Sorption and filtration of metals using iron-oxide-coated sand. *Water Res.* **30**, 2609–2620 (1996).
29. Marcogliese, D. J. *et al.* Effects of a major municipal effluent on the St. Lawrence River: A case study. *AMBIO* **44**, 257–274 (2015).
30. *Portrait global de l'état du Saint-Laurent 2024*. (Plan d'action Saint-Laurent 2011-2026, Québec, 2024).
31. Le Saint-Laurent - La qualité des eaux du fleuve, 1990-2003. https://www.environnement.gouv.qc.ca/eau/eco_aqua/fleuve/qualite90-03/index.htm?
32. Gregory, J. & Barany, S. Adsorption and flocculation by polymers and polymer mixtures. *Adv. Colloid Interface Sci.* **169**, 1–12 (2011).
33. Bolto, B. & Gregory, J. Organic polyelectrolytes in water treatment. *Water Res.* **41**, 2301–2324 (2007).
34. Lapointe, M. & Barbeau, B. Understanding the roles and characterizing the intrinsic properties of synthetic vs. natural polymers to improve clarification through interparticle Bridging: A review. *Sep. Purif. Technol.* **231**, 115893 (2020).
35. Torkzaban, S. & Bradford, S. A. Critical role of surface roughness on colloid retention and release in porous media. *Water Res.* **88**, 274–284 (2016).
36. Auset, M. & Keller, A. A. Pore-scale visualization of colloid straining and filtration in saturated porous media using micromodels. *Water Resour. Res.* **42**, 2005WR004639 (2006).
37. Das, S., Hendry, M. J. & Essilfie-Dughan, J. Transformation of Two-Line Ferrihydrite to Goethite and Hematite as a Function of pH and Temperature. *Environ. Sci. Technol.* **45**, 268–275 (2011).
38. Hiemstra, T. & Van Riemsdijk, W. H. Adsorption and surface oxidation of Fe(II) on metal (hydr)oxides. *Geochim. Cosmochim. Acta* **71**, 5913–5933 (2007).
39. Liu, H., Chen, T., Chang, J., Zou, X. & Frost, R. L. The effect of hydroxyl groups and surface area of hematite derived from annealing goethite for phosphate removal. *J. Colloid Interface Sci.* **398**, 88–94 (2013).
40. Kosmulski, M. The pH-Dependent Surface Charging and the Points of Zero Charge. *J. Colloid Interface Sci.* **253**, 77–87 (2002).
41. Mebarki, M., Joge Ngale, G. & Lapointe, M. Fibrous super-bridging agents simultaneously improve contaminants removal and sludge dewatering via a very compact three-in-one process. *Npj Clean Water* **8**, 11 (2025).

42. Iron - Contaminants in drinking water wells. *Gouvernement du Québec* https://www.quebec.ca/en/agriculture-environnement-et-ressources-naturelles/eau-potable/qualite-eau-potable/contaminants/effets-sante-contaminants/iron.
43. Abi Farraj, S. *et al.* Targeting nanoplastic and microplastic removal in treated wastewater with a simple indicator. *Nat. Water* **2**, 72–83 (2024).
44. Zhang, Y. *et al.* Aging significantly increases the interaction between polystyrene nanoplastic and minerals. *Water Res.* **219**, 118544 (2022).
45. Yao, K.-M., Habibian, M. T. & O'Melia, C. R. Water and waste water filtration. Concepts and applications. *Environ. Sci. Technol.* **5**, 1105–1112 (1971).
46. Tufenkji, N. & Elimelech, M. Correlation Equation for Predicting Single-Collector Efficiency in Physicochemical Filtration in Saturated Porous Media. *Environ. Sci. Technol.* **38**, 529–536 (2004).
47. Campos-Pereira, H. *et al.* The Adsorption of Per- and Polyfluoroalkyl Substances (PFASs) onto Ferrihydrite Is Governed by Surface Charge. *Environ. Sci. Technol.* **54**, 15722–15730 (2020).
48. Cogorno, J. & Rolle, M. Impact of Variable Water Chemistry on PFOS-Goethite Interactions: Experimental Evidence and Surface Complexation Modeling. *Environ. Sci. Technol.* **58**, 1731–1740 (2024).
49. Teymoorian, T. *et al.* A province-wide mapping of per- and polyfluoroalkyl substances (PFAS) in surface waters of the St. Lawrence River watershed, Québec, Canada. *Sci. Total Environ.* **1000**, 180429 (2025).
50. Kurusu, R. S., Lapointe, M. & Tufenkji, N. Sustainable iron-grafted cellulose fibers enable coagulant recycling and improve contaminant removal in water treatment. *Chem. Eng. J.* **430**, 132927 (2022).
51. Que-Trépanier, L., Victor, L. & Lapointe, M. Sustainable porous collectors for Agricultural Runoff Treatment. Preprint at https://doi.org/10.26434/chemrxiv-2025-r26fp (2025).
52. Albanakis, C., Tsanana, E. & Fragkaki, A. G. Modeling and prediction of trihalomethanes in the drinking water treatment plant of Thessaloniki, Greece. *J. Water Process Eng.* **43**, 102252 (2021).
53. Lapointe, M., Papineau, I., Peldszus, S., Peleato, N. & Barbeau, B. Identifying the best coagulant for simultaneous water treatment objectives: Interactions of mononuclear and polynuclear aluminum species with different natural organic matter fractions. *J. Water Process Eng.* **40**, 101829 (2021).

54. Parsada, L. A., Kamulyan, B. & Triatmadja, R. Study of Flow Rate Effect on Horizontal Flow Concrete Sand Filter Filtration Performance. *J. Civ. Eng. Forum* 23–30 (2023) doi:10.22146/jcef.6782.

55. Schreiber, B., Brinkmann, T., Schmalz, V. & Worch, E. Adsorption of dissolved organic matter onto activated carbon—the influence of temperature, absorption wavelength, and molecular size. *Water Res.* **39**, 3449–3456 (2005).

56. Kosmulski, M. pH-dependent surface charging and points of zero charge II. Update. *J. Colloid Interface Sci.* **275**, 214–224 (2004).

57. Effets sur la santé des contaminants de l'eau potable. *Gouvernement du Québec* https://www.quebec.ca/agriculture-environnement-et-ressources-naturelles/eau-potable/qualite-eau-potable/contaminants/effets-sante-contaminants.

58. Bai, R. & Zhang, X. Polypyrrole-Coated Granules for Humic Acid Removal. *J. Colloid Interface Sci.* **243**, 52–60 (2001).

59. Kosmulski, M. Isoelectric points and points of zero charge of metal (hydr)oxides: 50years after Parks' review. *Adv. Colloid Interface Sci.* **238**, 1–61 (2016).

60. Lapointe, M., Farner, J. M., Hernandez, L. M. & Tufenkji, N. Understanding and Improving Microplastic Removal during Water Treatment: Impact of Coagulation and Flocculation. *Environ. Sci. Technol.* **54**, 8719–8727 (2020).

61. Koumiya., Sauvé, S., Rochman, M. C., Lapointe, M. Intercepting contaminants in agricultural drainage water and runoff. (2025). *Communications Sustainability*.

62. Niarchos, G., Ahrens, L., Kleja, D. B. & Fagerlund, F. Per- and polyfluoroalkyl substance (PFAS) retention by colloidal activated carbon (CAC) using dynamic column experiments. *Environ. Pollut.* **308**, 119667 (2022).